CHEMISTRY
A EUROPEAN JOURNAL

Supporting Information

© Copyright Wiley-VCH Verlag GmbH & Co. KGaA, 69451 Weinheim, 2008

Zipped-up Chain-type Coordination Polymers: Unsymmetrical Amide-containing Ligands Inducing *b*-Sheet or Helical Structures

Kazuhiro Uemura,[a] Yuki Kumamoto,[b] and Susumu Kitagawa[b,c,d]

[a] *Environmental Science and Engineering, Graduate School of Science and Engineering, Yamaguchi University, Tokiwadai 2-16-1, Ube-shi, Yamaguchi 755-8611, Japan*.

[b] *Department of Synthetic Chemistry and Biological Chemistry, Graduate School of Engineering, Kyoto University, Katsura, Nishigyo-ku, Kyoto 615-8510, Japan*.

[c] *Institute for Integrated Cell-Material Sciences (iCeMS), Kyoto University, 69 Konoe-cho, Yoshida, Sakyo-ku, Kyoto 606-8501, Japan*.

[d] *ERATO Kitagawa Integrated Pore Project, Kyoto Research Park, Bldg#3, Shimogyo-ku, Kyoto, 600-8813, Japan*

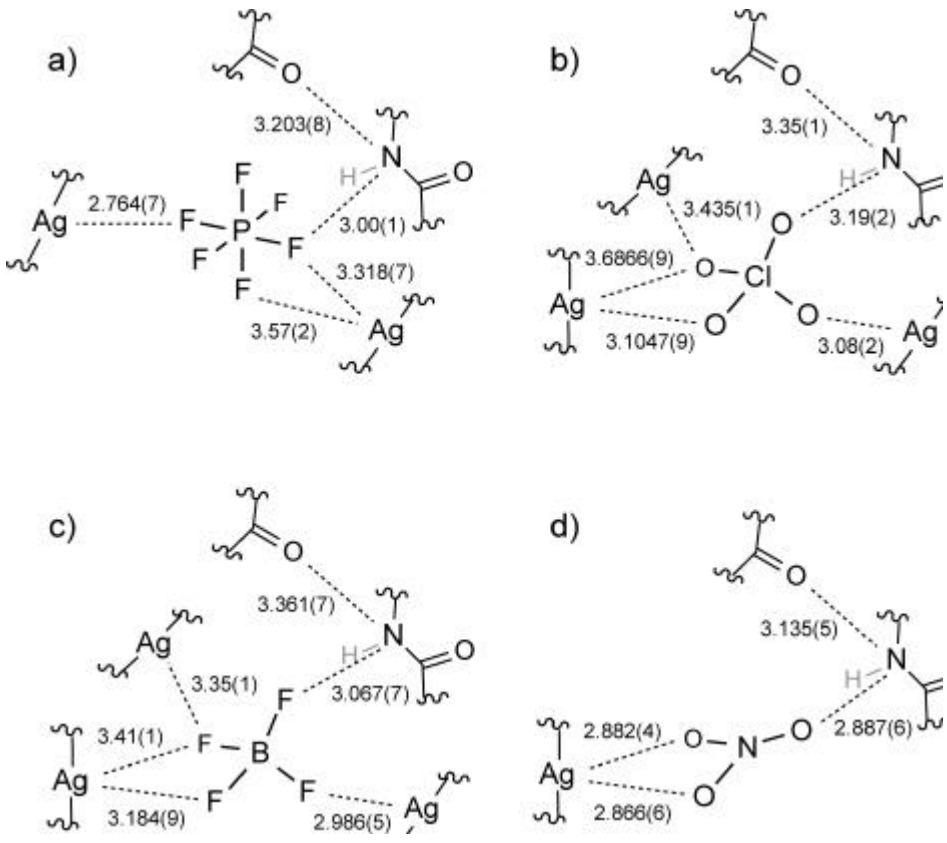

Figure S1. Schematic views of the anion environments in (a) {[Ag(4-pia)](PF$_6$)}$_n$ (**1** É **PF$_6^-$**), (b) {[Ag(4-pia)](ClO$_4$)}$_n$ (**1** É **ClO$_4^-$**), (c) {[Ag(4-pia)](BF$_4$)}$_n$ (**1** É **BF$_4^-$**) and (d)

{[Ag(4-pia)](NO$_3$)}$_n$ (**1** É **NO$_3^-$**). Numbers exhibit the distances (Å) among atoms. Expressions for double bonds in ClO_4^- and NO_3^- anions are omitted.

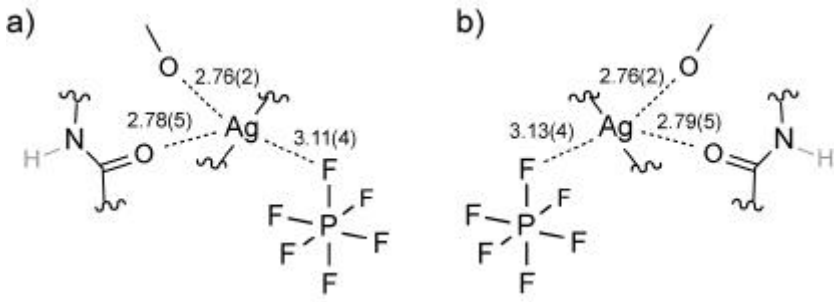

Figure S2. Schematic views of the PF_6^- environments in (a) {[Ag(4-pmna)](PF$_6$)·MeOH}$_n$ (**4a** É **PF$_6^-$·MeOH** and (b) {[Ag(4-pmna)](PF$_6$)·MeOH}$_n$ (**4b** É **PF$_6^-$·MeOH**). Numbers exhibit the distances (Å) among atoms.

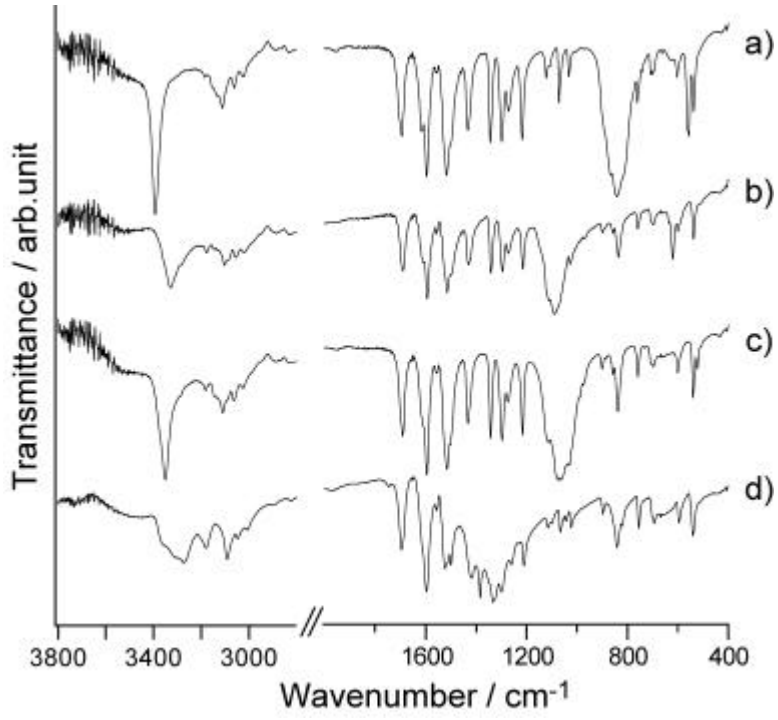

Figure S3. IR spectra of (a) {[Ag(4-pia)](PF_6)}$_n$ (**1** É **PF_6^-**), (b) {[Ag(4-pia)](ClO_4)}$_n$ (**1** É **ClO_4^-**), (c) {[Ag(4-pia)](BF_4)}$_n$ (**1** É **BF_4^-**) and (d) {[Ag(4-pia)](NO_3)}$_n$ (**1** É **NO_3^-**) at room temperature.

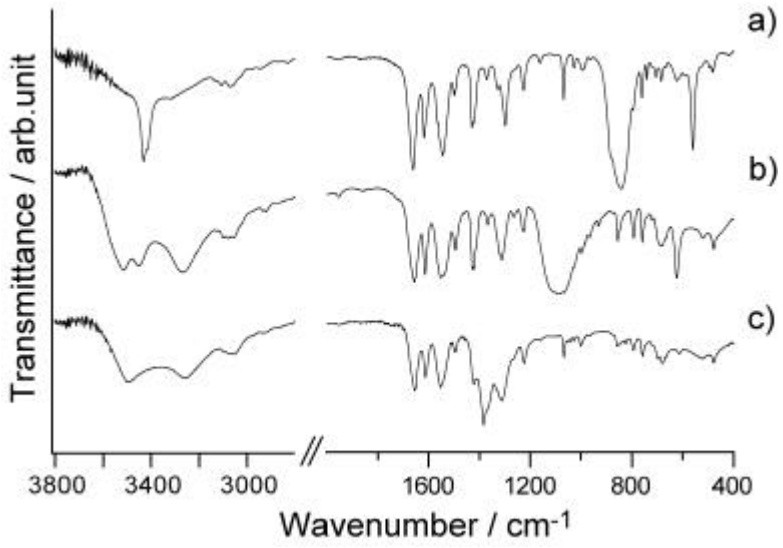

Figure S4. IR spectra of (a) {[Ag(4-pmia)](PF_6)}$_n$ (**2** É **PF_6^-**), (b) {[Ag(4-pmia)](ClO_4)·H_2O}$_n$ (**2** É **ClO_4^-·H_2O**) and (c) {[Ag(4-pmia)](NO_3)·H_2O}$_n$ (**2** É **NO_3^-·H_2O**) at room temperature.

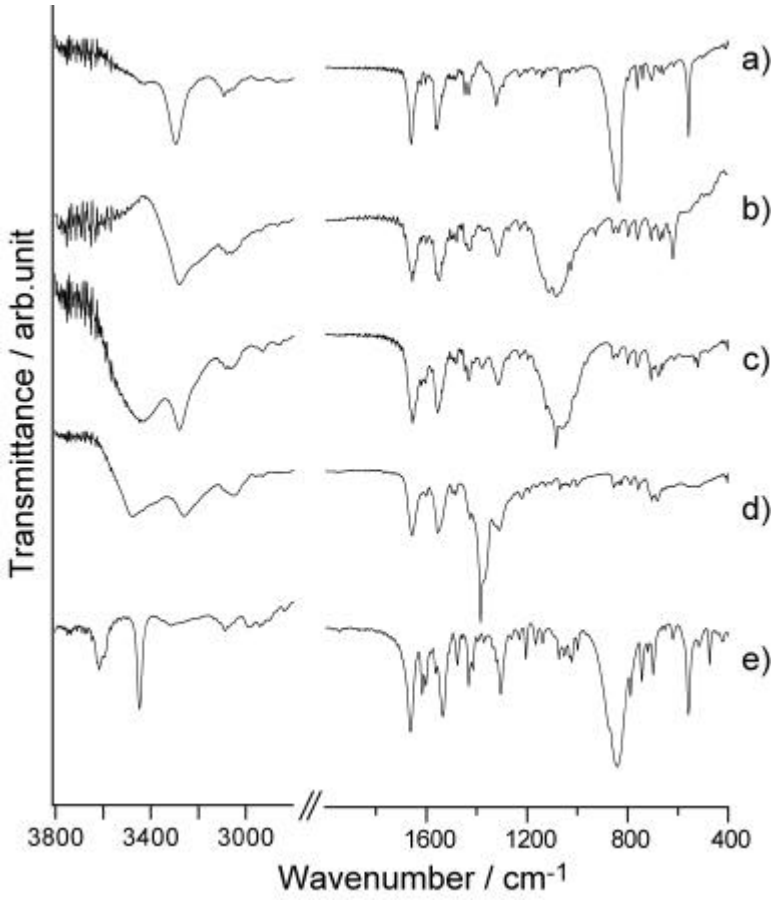

Figure S5. IR spectra of (a) {[Ag(3-pmia)](PF_6)}$_n$ (**3** É $\mathbf{PF_6^-}$), (b) {[Ag(3-pmia)](ClO_4)}$_n$ (**3** É $\mathbf{ClO_4^-}$), (c) {[Ag(3-pmia)](BF_4)}$_n$ (**3** É $\mathbf{BF_4^-}$), (d) {[Ag(3-pmia)](NO_3)·H_2O}$_n$ (**3** É $\mathbf{NO_3^-{\cdot}H_2O}$)

and (e) {[Ag(4-pmna)](PF_6)·MeOH}$_n$ (**4** É **PF_6^-·MeOH**) at room temperature.

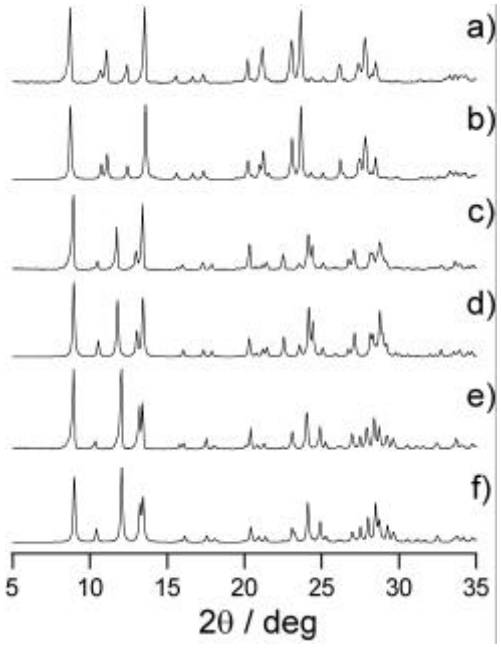

Figure S6. XRPD patterns of (a) as prepared {[Ag(4-pia)](PF_6)}$_n$ (**1** É **PF_6^-**), (b) simulation of **1** É **PF_6^-**, (c) as prepared {[Ag(4-pia)](ClO_4)}$_n$ (**1** É **ClO_4^-**), (d) simulation of **1** É **ClO_4^-**, (e) as prepared {[Ag(4-pia)](BF_4)}$_n$ (**1** É **BF_4^-**) and (f) simulation of **1** É **BF_4^-**. Since it was not succeeded in obtaining the microcrystalline sample **1** É **NO_3^-**, single crystals were used for some experiments. The simulation patterns were based on the single X-ray analyses.

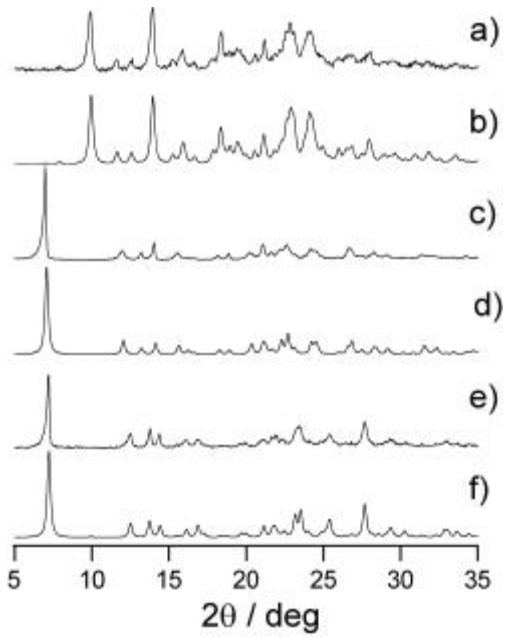

Figure S7. XRPD patterns of (a) as prepared $\{[Ag(4\text{-pmia})](PF_6)\}_n$ (**2** É $\mathbf{PF_6^-}$), (b) simulation of **2** É $\mathbf{PF_6^-}$, (c) as prepared $\{[Ag(4\text{-pmia})](ClO_4)\cdot H_2O\}_n$ (**2** É $\mathbf{ClO_4^-\cdot H_2O}$), (d) simulation of **2** É $\mathbf{ClO_4^-\cdot H_2O}$, (e) as prepared $\{[Ag(4\text{-pmia})](NO_3)\cdot H_2O\}_n$ (**2** É $\mathbf{NO_3^-\cdot H_2O}$) and (f) simulation of **2** É $\mathbf{NO_3^-\cdot H_2O}$. The simulation patterns were based on the single X-ray analyses.

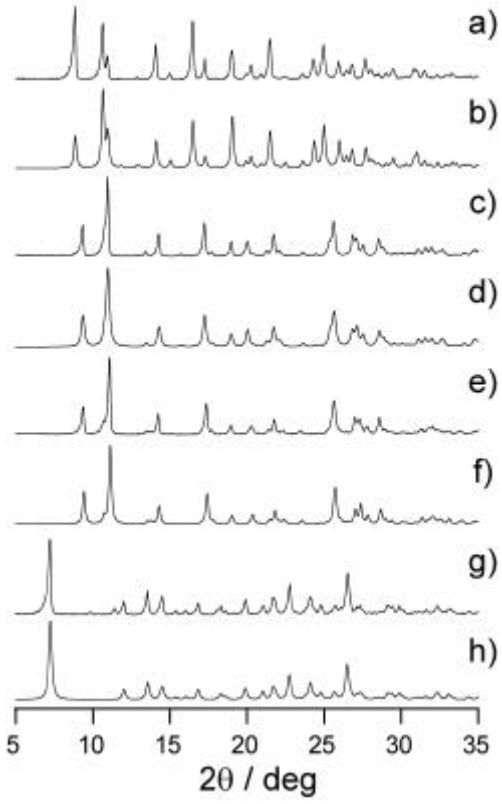

Figure S8. XRPD patterns of (a) as prepared $\{[Ag(3\text{-pmia})](PF_6)\}_n$ (**3** É $\mathbf{PF_6^-}$), (b) simulation of **3** É $\mathbf{PF_6^-}$, (c) as prepared $\{[Ag(3\text{-pmia})](ClO_4)\}_n$ (**3** É $\mathbf{ClO_4^-}$), (d) simulation of **3** É $\mathbf{ClO_4^-}$, (e) as prepared $\{[Ag(3\text{-pmia})](BF_4)\}_n$ (**3** É $\mathbf{BF_4^-}$), (f) simulation of **3** É $\mathbf{BF_4^-}$, (g) as prepared $\{[Ag(3\text{-pmia})](NO_3)\cdot H_2O\}_n$ (**3** É $\mathbf{NO_3^-\cdot H_2O}$) and (h) simulation of **3** É $\mathbf{NO_3^-\cdot H_2O}$. The simulation patterns were based on the single X-ray analyses.

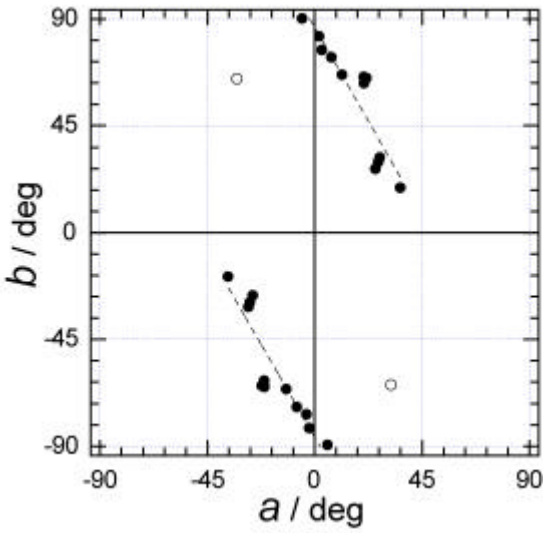

Figure S9. The plots of *b* versus *a*. Open circles are corresponding to those in $\{[Ag(4\text{-pmia})](PF_6)\}_n$ (**2** É $\mathbf{PF_6^-}$). Other angles (filled circles) appear a tendency for a large value of *a* to be accompanied by a small value of *b*.

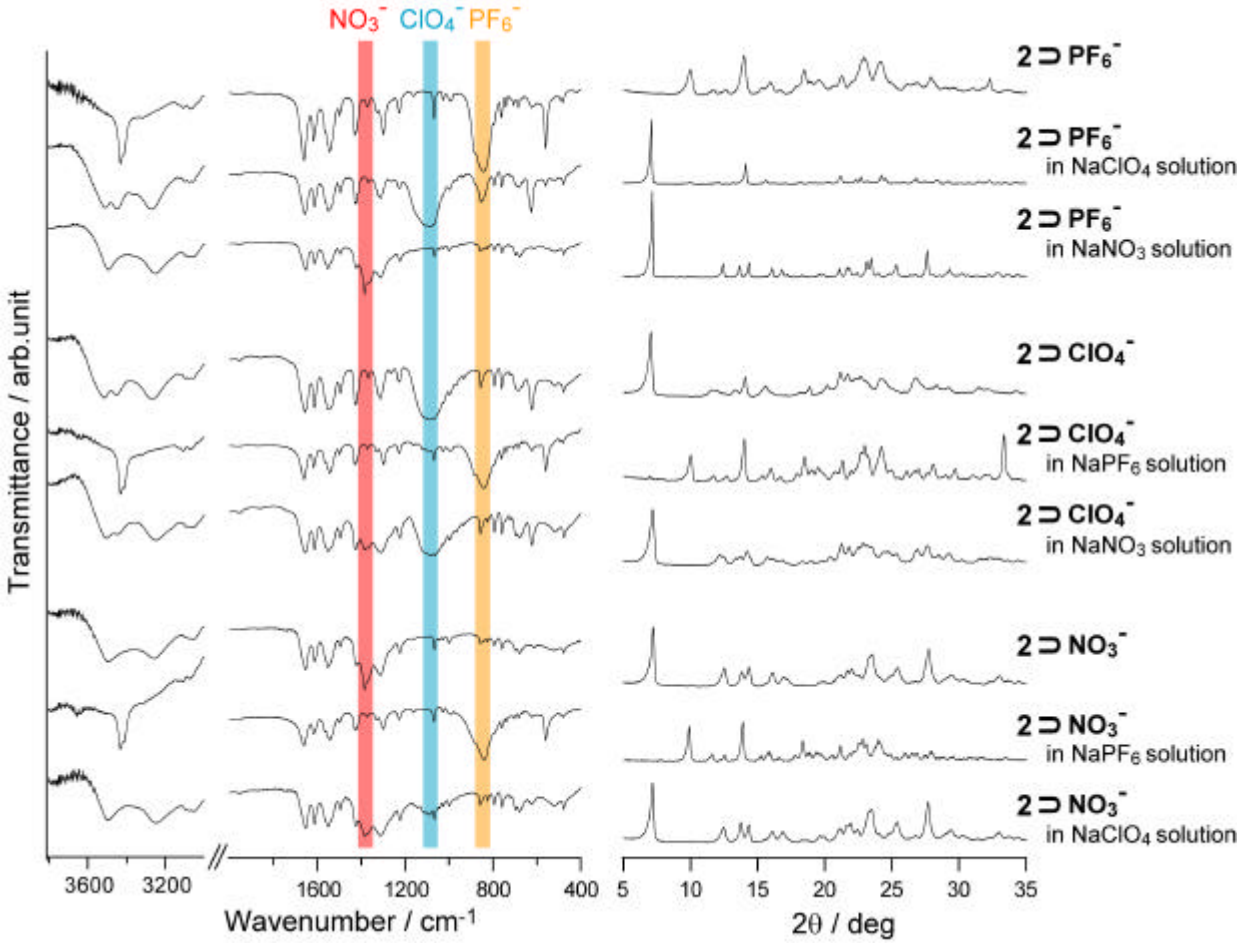

Figure S10. XRPD patterns (left) and IR spectra (right) at room temperature for anion exchange of compounds **2**. See the text for the detailed information.

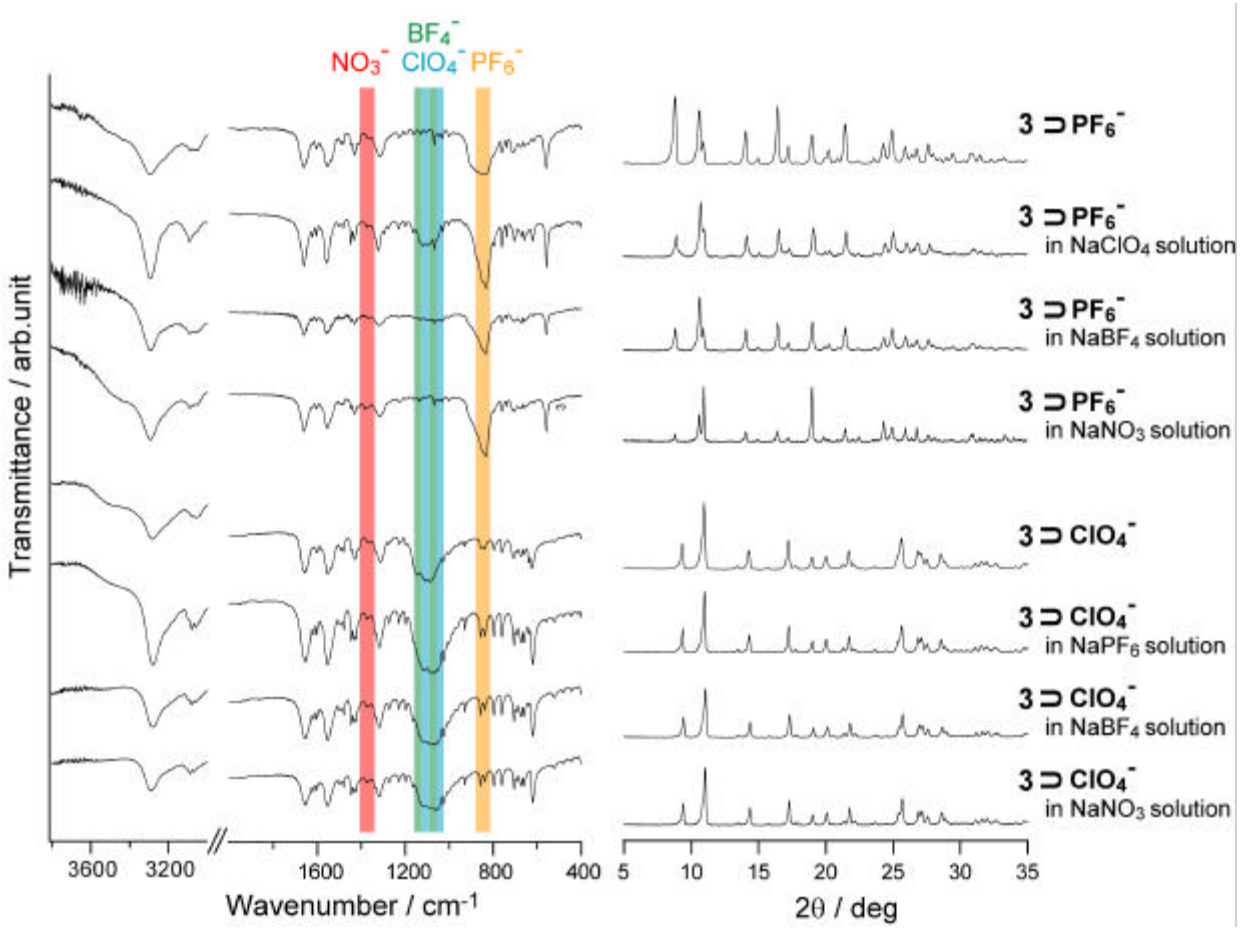
BF4-
NO3- ClO4- PF6-
Transmittance / arb.unit
3600
3200
1600
1200
800
400
Wavenumber / cm-1
3 ⊃ PF6-
3 ⊃ PF6- in NaClO4 solution
3 ⊃ PF6- in NaBF4 solution
3 ⊃ PF6- in NaNO3 solution
3 ⊃ ClO4-
3 ⊃ ClO4- in NaPF6 solution
3 ⊃ ClO4- in NaBF4 solution
3 ⊃ ClO4- in NaNO3 solution
5
10
15
20
25
30
35
2θ / deg

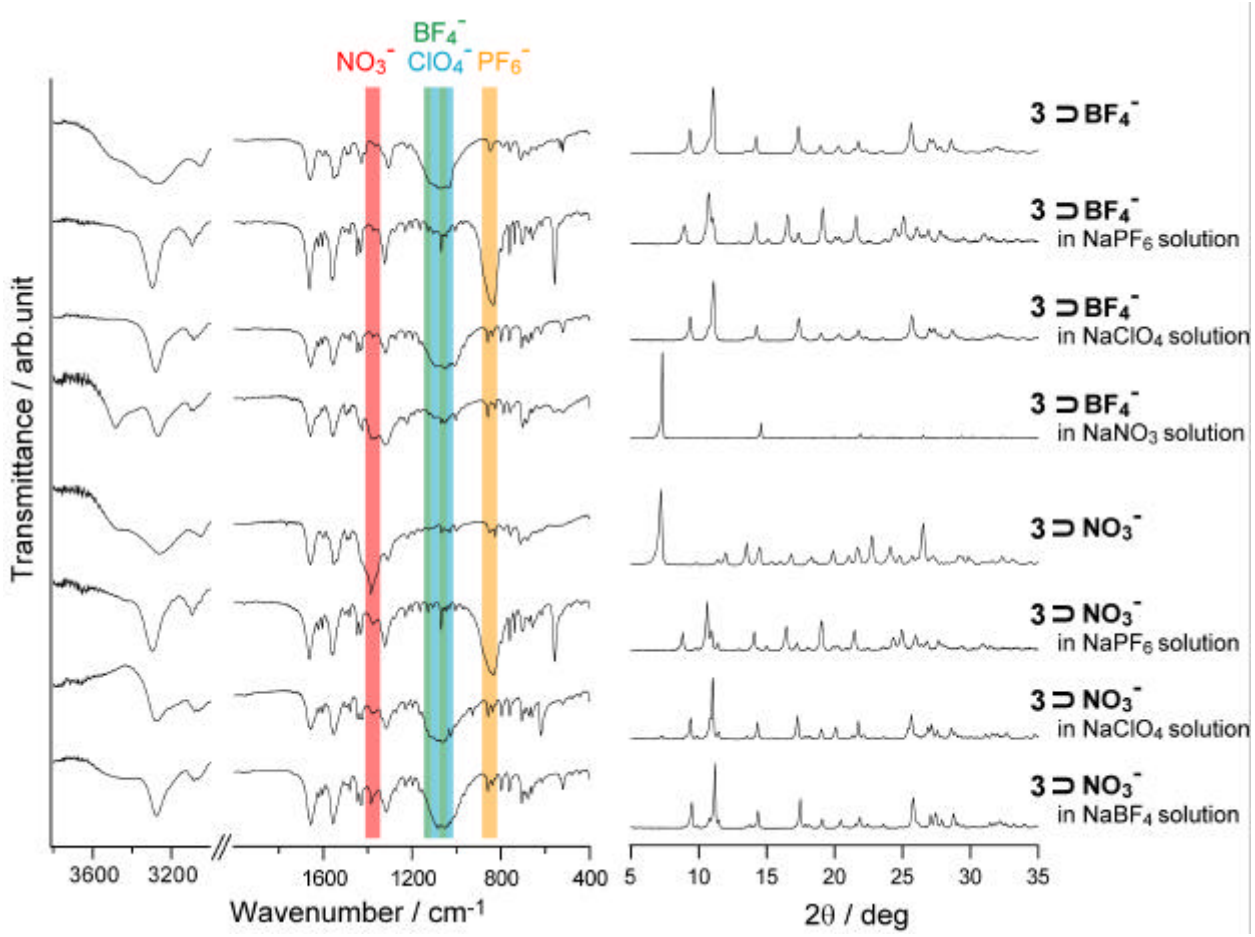

Figure S11. XRPD patterns (left) and IR spectra (right) at room temperature for anion exchange of compounds **3**. See the text for the detailed information.